Nuclear Science and Techniques (2023) 34:144
https://doi.org/10.1007/s41365-023-01297-x

EJUSTCO: Monte Carlo radiation transport code hybrid with ANN model for gamma-ray shielding simulation

Joseph Konadu Boahen[1] · Ahmed S. G. Khalil[2] · Mohsen A. Hassan[1] · Samir A. Elsagheer Mohamed[3]

Received: 1 September 2022 / Revised: 15 June 2023 / Accepted: 18 June 2023 / Published online: 29 September 2023

Abstract

Gamma ray shielding is essential to ensure the safety of personnel and equipment in facilities and environments where radiation exists. The Monte Carlo technique is vital for analyzing the gamma-ray shielding capabilities of materials. In this study, a simple Monte Carlo code, EJUSTCO, is developed to cd simulate gamma radiation transport in shielding materials for academic purposes. The code considers the photoelectric effect, Compton (incoherent) scattering, pair production, and photon annihilation as the dominant interaction mechanisms in the gamma radiation shielding problem. Variance reduction techniques, such as the Russian roulette, survival weighting, and exponential transformation, are incorporated into the code to improve computational efficiency. Predicting the exponential transformation parameter typically requires trial and error as well as expertise. Herein, a deep learning neural network is proposed as a viable method for predicting this parameter for the first time. The model achieves an MSE of 0.00076752 and an R-value of 0.99998. The exposure buildup factors and radiation dose rates due to the passage of gamma radiation with different source energies and varying thicknesses of lead, water, iron, concrete, and aluminum in single-, double-, and triple-layer material systems are validated by comparing the results with those of MCNP, ESG, ANS-6.4.3, MCBLD, MONTEREY MARK (M), PENELOPE, and experiments. Average errors of 5.6%, 2.75%, and 10% are achieved for the exposure buildup factor in single-, double-, and triple-layer materials, respectively. A significant parameter that is not considered in similar studies is the gamma ray albedo. In the EJUSTCO code, the total number and energy albedos have been computed. The results are compared with those of MCNP, FOTELP, and PENELOPE. In general, the EJUSTCO-developed code can be employed to assess the performance of radiation shielding materials because the validation results are consistent with theoretical, experimental, and literary results.

Keywords Monte Carlo · Gamma rays · Shielding · Artificial neural network · Simulation

1 Introduction

Ionizing radiation, such as gamma radiation, traverses through matter and changes the material structure upon interaction with matter. In biological systems and electronic devices for space exploration and signaling, exposure to radiation can cause damage or injury; thus, adequate protection is necessitated [1]. Understanding the manner by which gamma rays interact with a material to reduce its intensity is essential for providing adequate shielding. The photon intensities are reduced through photoelectric absorption, Compton scattering, pair production, and coherent scattering interactions [2, 3], which are explained in detail in the Sect. 2 herein. Computational techniques are used to analyze the transport of photons through matter. The computational methods used to analyze photon transport in materials can

✉ Joseph Konadu Boahen
joseph.boahen@ejust.edu.eg

Mohsen A. Hassan
mohsen.khozami@ejust.edu.eg

[1] Materials Science and Engineering Department, School of Innovative Design Engineering, Egypt-Japan University of Science and Technology (E-JUST), 179, New Borg El-Arab City, Egypt

[2] Physics Department, Environmental and Smart Technology Group, Faculty of Science, Fayoum University, Fayoum 63514, Egypt

[3] Faculty of Engineering, Aswan University, Aswan, Egypt

be regarded as deterministic, such as the discrete ordinate, finite element, point kernel, or statistical methods, which house the Monte Carlo method [4]. The Monte Carlo method is considered the preferred method to simulate gamma radiation penetration through matter as it considers the physical nature of the interaction process and allows intractable results using experiments to be obtained computationally [5, 6]. Consequently, the Monte Carlo method has been used to benchmark against other methods. Commercial computer codes developed based on the Monte Carlo technique include GEANT 4, MCNP, and EGS4 [7–9]. However, students cannot easily access these codes for shielding analysis because most of them are not open-source codes; in some cases, location can limit access to such codes, and the usage of these codes requires considerable expertise, which can be overwhelming for students, particularly undergraduates. Hence, a simple Monte Carlo code, EJUSTCO, is developed in this study for academic and research purposes, with emphasis on graduate and undergraduate students. The program is written in MATLAB, which allows the algorithm to be implemented, debugged, and tested easily. In addition, the code employs gamma-ray cross-sectional data from the XCOM database, which are easier to assess and incorporate into the code compared with other sources used in other codes. Herein, validation results of the code based on the dose rate, exposure buildup factor, and radiation albedos as quantities of interest are presented [10, 11]. The total energy and number albedos are computed for water and aluminum in the energy range of 20–100 keV. The obtained albedo values are validated using results from general-purpose codes MCNP, FOLTELP, and PENELOPE. The developed code is used to analyze the exposure buildup factor and the dose rate of common shielding materials, such as lead, aluminum, water, iron, and concrete. The materials are considered single-, double-, and triple-layered systems. A comparison of the simulation results for the dose rate and buildup factor with results from codes such as MCNP, EGS4, GP, and ANSI-6.4.3, PENELOPE, and the literature is performed to validate the EJUSTCO code. To achieve reliable results, an exponential transformation variance technique is employed to ensure that the particles reach deeper regions of the shield. However, determining the arbitrary parameters used in this technique, which are typically obtained through trial and error, is challenging. Hence, in this study, we investigate the prospects of using artificial neural networks (ANNs) to predict the arbitrary parameters by training the generated data. ANNs are preferred because they have been shown to effectively predict values when the general trends of such parameters are unknown; furthermore, ANNs are suitable for any function, at least theoretically [12]. Thus, by training the available data, the ANN model can fit the data to obtain a general model that can predict values without trial and error. Based on the unique advantages of neural networks [13–15], an ANN model is developed to predict exponential transformation parameters. In all validations, the developed code agrees well with the experimental results, thus demonstrating the significant potential of ANNs. Additionally, the ANN model is a practical example where current techniques can be employed in conjunction with conventional methods. In the developed code, photon tracks and the position where gamma rays deposit their energies can be generated, thus allowing students to visually appreciate the transport process within the medium. The remainder of this paper is organized as follows: the Monte Carlo procedure is described in Sect. 2, the general algorithm is provided in Sect. 3, the results and discussion are presented in Sect. 4, and the conclusion is presented in Sect. 5.

2 Problem investigated and calculation procedure

The Monte Carlo simulation of photon transport involves several histories of photons from birth to death and requires the sampling of various physical parameters that govern the trajectory of photons through the medium. A photon begins its journey in a medium by assigning its initial position and direction. The photon traverse a certain distance, which is referred to as the photon path length, before interacting with a medium. This distance is sampled using the energy-dependent total cross-section of the medium, within which the photon traverses. Once a collision site is reached, the photons interact with the medium through different mechanisms. The interaction type is selected using individual and total cross-sections (interaction probabilities). Relevant information regarding the photons at the collision site is stored for further processing. This process continues until the photon's history is terminated using several cutoff techniques such as energy, weight (in an automated Monte Carlo method), and time. For this process to be successful, a random number generator must be employed, which is the core of the simulation process. In this study, the rand function in MATLAB is used as a random number generator to generate random numbers between (0,1) from the canonical probability distribution. The following subsections briefly explain the interaction mechanisms and mathematical models underlying this procedure.

2.1 Interaction mechanisms

The photoelectric absorption effect is an interaction mechanism in which the gamma ray provides all its energy to a bound electron, as depicted in Fig. 1a. In this process, some of the energy overcomes the binding energy of a bound electron, and the free electron absorbs the remaining photon energy in the form of kinetic energy. Only a small portion

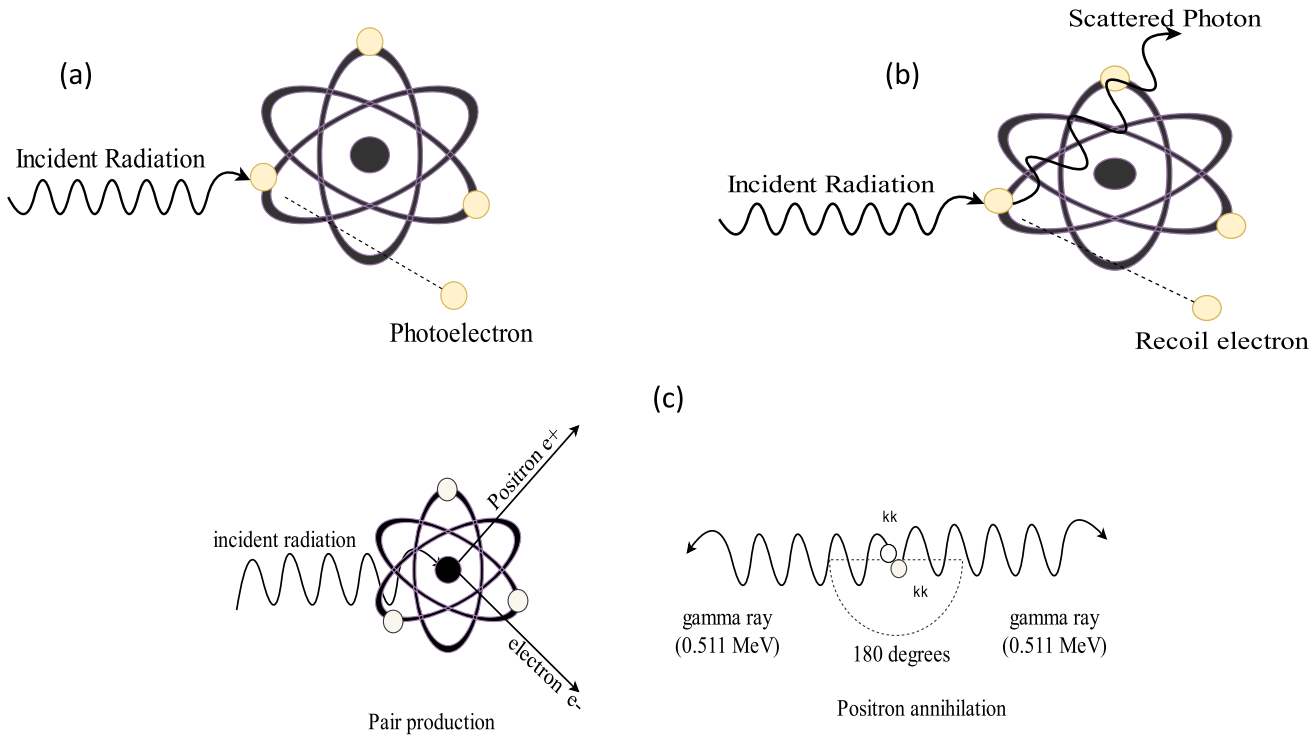

Fig. 1 **a** Photoelectric effect; **b** Compton scattering; **c** pair production and annihilation of positrons and electrons

of energy remains in the atom to conserve momentum [16, 17]. Gamma rays can be scattered when they interact with a bound electron through Compton scattering, which consequently changes the photon direction and energy. Additionally, the bound electrons gain kinetic energy. After the interaction, the energy of the secondary photon due to scattering as a function of the scattering angle θ is computed using Eq. (1).

$$E_{\gamma'} = \frac{E_\gamma}{1 + \frac{E_\gamma}{mc^2}(1 - \cos\theta)} \tag{1}$$

The Compton scattering mechanism is illustrated schematically in Fig. 1b. Pair production involves the total absorption of the primary gamma ray and the generation of an electron–positron pair with kinetic energies, as expressed in Eq. (2).

$$T_{e^-} + T_{e^+} = E_\gamma - 1.022\,\text{MeV}, \tag{2}$$

where T_{e^-} and T_{e^+} are the kinetic energies of the electron and positron, respectively.

Based on Eq. (2), the threshold energy for pair production is above 1.022 MeV. After a pair is created, the positron annihilates to release two photons of 0.511 MeV energy each and traverses 180° opposite each other. This mechanism is illustrated in Fig. 1c. Typically, the annihilated photons are followed individually while they are traversing 180° apart and are considered the classical model in this work. However, a strategy that can reduce computational time yet exhibits an extremely small error has been suggested previously; in this strategy, only one photon with an energy of 0.511 MeV is followed, and its weight is compensated by 2. This approach was considered a simple model [18]. The two strategies mentioned above were investigated to ascertain their accuracy.

2.2 Photon path length and scoring

The photon is transported through a medium by sampling the path length to a collision site from the exponential distribution, which can be expressed as follows:

$$p(s) = \mu e^{-\mu s}, \quad 0 \le s \le \infty, \tag{3}$$

where $e^{-\mu s}$ is the probability of a gamma ray traveling a distance s without interaction. Thus, the probability that a gamma ray will interact in the interval ds is μ ds. Therefore, the probability of a gamma ray interacting between distance s and $s+$ds by $\mu e^{\mu s}$ds can be expressed as

$$\mu \int_0^s e^{-\mu s}\,\mathrm{d}s = \int_0^\xi \mathrm{d}y \Rightarrow 1 - e^{-\mu s} = \xi. \tag{4}$$

Hence, the path length can be calculated as shown in Eq. (5).

$$s = -\frac{1}{\mu}\ln(1-\xi) = -\frac{1}{\mu}\ln\xi \tag{5}$$

Here, ξ is a random number governed by the canonical distribution $[p(\xi) = 1,\ 0 \le \xi \le 1]$. Herein, μ is the total gamma photon attenuation coefficient that describes the probability of the photon undergoing an interaction; mathematically, it is the sum of the individual cross-sections of the interactions. For this code, all photon cross-sections were obtained using XCOM [19]. A graphical representation of the various gamma interaction cross-sections for the materials investigated in the study is shown in Fig. 2.

The quantities of importance in the code, namely the dose rate, photon exposure buildup factor, and albedo, were calculated using a surface crossing estimator [20]. The estimator for a particle with energy ΔE_i in volume ΔV_i is expressed as

$$C(i,j) = C(i,j) + w \times l, \tag{6}$$

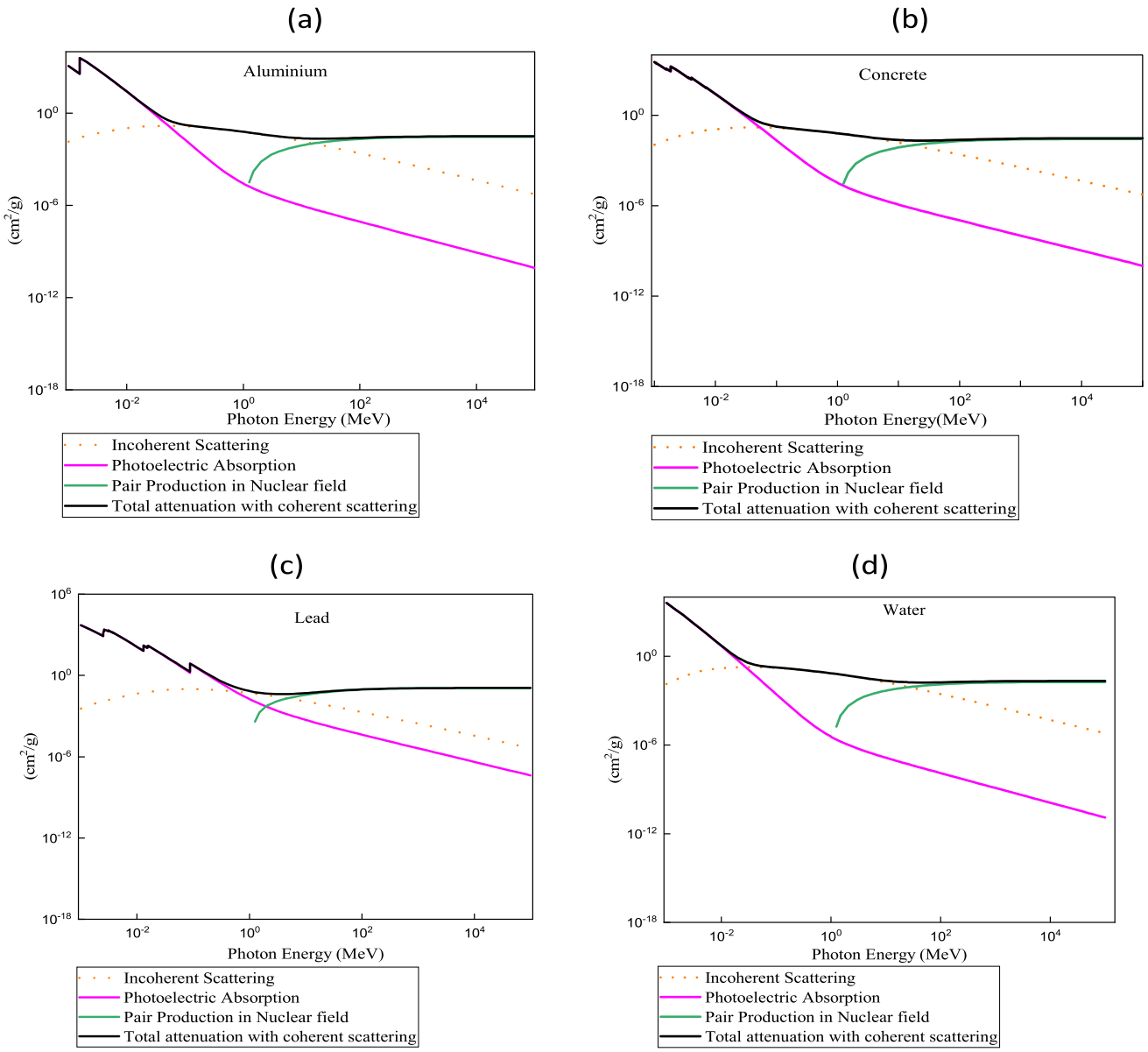

Fig. 2 (Color online) Gamma interaction cross-section variation with energy in **a** aluminum, **b** concrete, **c** lead, and **d** water

$$C(i,j) = C(i,j) + w \times \frac{\Delta x_i}{|\cos\theta|}, \tag{7}$$

where $C(i,j)$ is the counter, w the weight of the particle, and l the path length inside the volume ΔV_i. The projection along the thickness is expressed as $\frac{\Delta x_i}{|\cos\theta|}$, as shown in Eq. (7). The absolute sign is considered to include all particles moving in all directions. When the absolute value approaches $\cos\theta = 0$, a value of 0.005 is assigned to prevent the estimator from becoming indeterminate. By specifying Δx_i as unity, the scalar flux for energy j outside a particular surface can be expressed as

$$\varphi(E_j) = \varphi(E_j) + w \times \frac{1}{|\cos\theta|}. \tag{8}$$

2.3 Translation and rotation of photon

After the tentative path length is calculated using Eq. (5), the photon traverses to the next interaction site via coordinate transformation and rotation. The new position of the gamma ray after an interaction (x,y,z) in the direction $\overrightarrow{u_0} = (u_0, v_0, w_0) = (\sin\theta\cos\varphi,\ \sin\theta\sin\varphi,\ \cos\theta)$ can be computed using Eq. (9).

$$\vec{x} = \vec{x}_0 + \vec{u}_0 s \Rightarrow \begin{cases} x = x_0 + u_0 s \\ y = y_0 + v_0 s \\ z = z_0 + w_0 s \end{cases} \tag{9}$$

Next, we introduce the rotation matrix $R(\theta,\varphi)$ Eq. (10) as follows:

$$R(\theta,\varphi) = \begin{pmatrix} \cos\theta\cos\varphi & -\sin\varphi & \sin\theta\cos\varphi \\ \cos\theta\sin\varphi & \cos\varphi & \sin\theta\sin\varphi \\ -\sin\theta & 0 & \cos\theta \end{pmatrix} \tag{10}$$

The function of the rotation matrix $R(\theta,\varphi)$ is to transform the gamma-ray vector components from the local coordinates to the laboratory coordinate system (x,y,z) via the azimuthal angle φ about the positive z-axis, followed by the rotation of the polar angle θ about y' [21]. After the transformation, the three components of the new direction cosine, namely u, v, and w are calculated using Eq. (11).

$$\begin{aligned} u &= \sin\theta\cos\varphi = u_0\cos\theta + \sin\theta\left(w_0\cos\phi\cos\varphi_0 - \sin\phi\sin\varphi_0\right) \\ v &= \sin\theta\sin\varphi = v_0\cos\theta + \sin\theta\left(w_0\cos\phi\sin\varphi_0 + \sin\phi\cos\varphi_0\right) \\ w &= \cos\theta = w_0\cos\theta - \sin\theta\sin\theta_0\cos\phi \end{aligned} \tag{11}$$

Using the aforementioned methodologies, the entire gamma-ray trajectory can be described. Each particle is monitored from birth until any cutoff condition terminates its life history or until it escapes from the medium. During particle transport, sampling is performed using known probability density functions for different physical processes. For double- and triple-layer systems, surface-to-surface tracking [22] accounts for boundary crossing and regional changes in an event in which a photon leaves its current region for a new one.

2.4 Variance reduction (Biasing)

Variance is used to increase the efficiency and computational speed. The developed code applies the survival weight, exponential transform, and Russian roulette. The survival weight prevents the direct absorption of the particles by inducing forced scattering. This technique increases the number of photons that can penetrate important areas, thereby increasing the particle score in significant regions of the medium prior to premature absorption. The survival-weight technique is essential for shielding applications involving thick media. The introduced bias is mitigated by adjusting the particle weight after each collision by multiplying the photon survival weight by a factor, as shown in Eq. (12).

$$w = w_{\mathrm{O}}\frac{\sigma_c}{\mu}, \tag{12}$$

where the ratio $\frac{\sigma_c}{\mu}$ is the probability of a scattering event.

The photon is assigned a weight of unity from the source, i.e., $w_{\mathrm{O}} = 1$, which is adjusted as the simulation proceeds [14]. The exponential transform performs a function similar to the survival weight. However, this technique improves the particle score by increasing the path length of the photon when it approaches a region of interest (ROI), i.e., where scoring is desired.versely, the particle path length is reduced when the particle departs from the ROI. The exponential transformation is executed by replacing the actual total cross-section μ with a transformed total cross-section μ'. expressed as $\mu' = \mu - cu.$, which is dependent on the direction, or $\mu' = \mu * c$, which is the direction-independent transformed total cross-section [23]. In this code, the latter is employed because the directional form introduces fluctuations in the computation of the buildup factor. Subsequently, the path length is sampled using the transformed total cross-section as follows:

$$s = \frac{-\ln(\xi)}{\mu'} \Rightarrow \frac{-\ln(\xi)}{\mu * c}. \tag{13}$$

The weights of the particles are adjusted accordingly to remove the effect of bias as follows:

$$w = \frac{w_{\mathrm{O}}}{c} e^{[-s\mu(1-c)]}. \tag{14}$$

When $c > 1$, the path length is reduced and is typically used in situations where buildup zones exist at the medium entrance. If $c = 1$, then sampling is performed using the untransformed total cross-section; meanwhile, if $0 < c < 1$, then the path length is stretched, which renders its applicable to thick media. This technique is useful for shielding problems in which the particle history is terminated before detection, which is characteristic of deep penetration problems.

The Russian roulette determines whether a particle's life history must be terminated or continued when its weight is low. This technique is typically used to prolong the computational time. A particle is assigned a probability of survival, e.g., 1 out of 10. If a generated random number exceeds 0.1, then the history is terminated and the particle history continues [14].

2.5 ANN

As mentioned previously, obtaining an arbitrary parameter for the exponential transformation involves trial and error. Once data are available for parameters that require trial and error, such data can be trained using machine-learning techniques, such as ANNs, to predict such parameters. An ANN is based on the manner in which the human brain processes information using neurons. A typical ANN contains neurons, which are known as nodes, that are connected to form a web-like system. Additionally, an ANN comprises an input layer that receives input data and transmits it through a hidden layer, if such a layer exists. Finally, an output is produced after data processing is performed [24]. An ANN can be considered a perceptron if it does not contain any hidden layers, a multilayer perceptron if it comprises three layers, or a deep neural network if it comprises more than three hidden layers [25]. Deep learning is desirable owing to its high precision [26]. In this study, an ANN model, i.e., a deep neural network, is proposed to predict the exponential transformation parameter c. The proposed model is shown in Fig. 3.

The input data are transmitted between the hidden layers using a transfer function, which is expressed as

$$H_j = \sum_{i=1}^{n} w_i^{\mathrm{T}} x_i + b$$

Here, H_j is the input to the next layer and w_i^{T} is the weight of the ith x_i input. The sum of the weights generates activation, which is the signal strength. After processing the output using the hidden layers, the output is generated using an activation function that can be a linear or nonlinear function, such as a sigmoidal hyperbolic function, expressed as

$$f(x) = 1/\left[1 + \exp\left(-x_i\right)\right]. \tag{15}$$

Subsequently, the output returned in the output layer is

$$y_j = 1/\left[1 + \exp\left(-H_j\right)\right]. \tag{16}$$

Because ANNs are machine-learning techniques, the network must be trained before deployment. In this context, the suitable learning schemes include the Newton, quasi-Newton, Conjugate gradient, gradient descent, and Levenberg–Marquardt schemes. The detailed algorithms of these schemes are not presented here as they are available in [27].

2.5.1 Network properties

For the developed ANN, the input parameters were the material density and radiation energy, and the output is the parameter c. The simulation results obtained from EJUSTCO after validation were used as the dataset required to train the network. The network was trained using the Levenberg–Marquardt algorithm [28]. The numbers of samples for training and validating the model

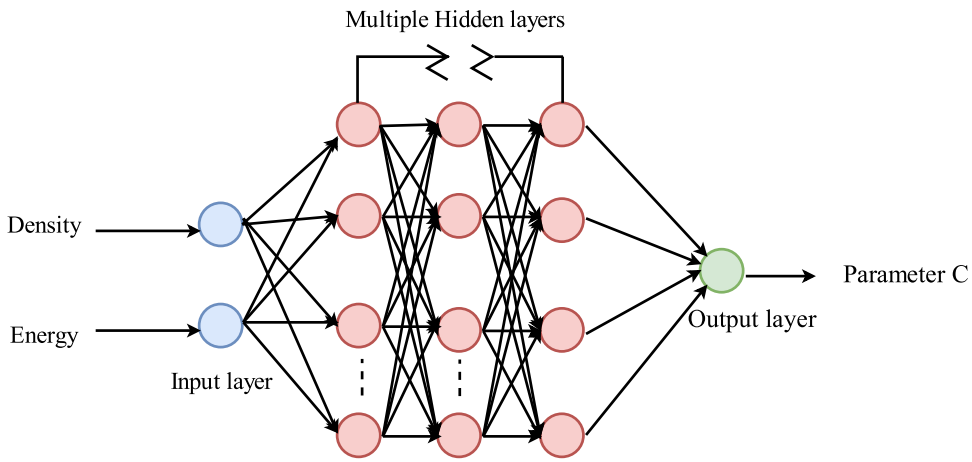

Fig. 3 The proposed deep neural network architecture

were 34 (60%) and 22 (40%), respectively. The MATLAB R2022a software was used to train the ANN model. To obtain the optimum configuration in terms of the number of hidden layers, an intrinsic MATLAB machine-learning optimization tool for selecting the hyperparameters, i.e., Bayesopt, which is based on Bayesian optimization, was employed.

2.6 Dose rate, exposure buildup factor, and albedo evaluation

After all histories have been simulated, the code computes quantities that characterize the shield's performance by evaluating all tallies corresponding to each. The dose rate provides a quantitative measure of the radiation risk at a point behind the shield and provides information regarding the hazards posed by radiation. The code evaluates the dose rate as follows:

$$\text{Dose} = \sum_{g=1}^{G} \varphi(r,E)\cdot K\cdot \bar{E}_g \cdot \frac{\mu_{\text{en}}^{\text{air}}\left(\bar{E}_g\right)}{\rho}, \tag{17}$$

where $\varphi(r,E)$ is the total photon flux at a distance r, K the dose conversion factor, $\overline{E}_g$ the average photon energy, and $\frac{\mu_{\text{en}}^{\text{air}}\left(\overline{E}_g\right)}{\rho}$ the energy absorption coefficient of air at energy $\overline{E}_g$. The dose is the total dose at a point comprising both scattered and noncollided photons.

The exposure buildup factor is evaluated as the ratio of the total dose to the uncollided dose and is expressed as

$$EBF = \frac{\sum_{g=1}^{G} \varphi_g \cdot \overline{E}_g \cdot \frac{\mu_{\text{en}}^{\text{air}}\left(\overline{E}_g\right)}{\rho}}{\varphi_u \cdot E_0 \frac{\mu_{\text{em}}^{\text{air}}\left(\overline{E}_g\right)}{\rho}}. \tag{18}$$

Here, φ_u is the uncollided photon flux defined by Beer and Lambert, which is expressed as $\varphi_u = \varphi_0 \exp(-\mu r) = \left(S/4\pi r^2\right)\exp(-\mu r)$; and φ_0 is the total photon history based on the initial photon flux impinging on the material surface.

The integration of the differential albedo generally computes the total albedo over energy and the solid angle for the directional domain as a function of both the total number and energy albedos as follows:

$$a_N\left(E_0,\theta_0\right) = \int_0^{E_0} \mathrm{d}E \int_0^{2\pi} \mathrm{d}\varphi \int_0^{\pi/2} a\left(E_0,\theta_0;E,\theta,\varphi\right)\sin\theta \mathrm{d}\theta, \tag{19}$$

$$a_E\left(E_0,\theta_0\right) = \frac{1}{E_0}\int_0^{E_0} E\mathrm{d}E \int_0^{2\pi} \mathrm{d}\varphi \int_0^{\pi/2} a\left(E_0,\theta_0;E,\theta,\varphi\right)\sin\theta \mathrm{d}\theta. \tag{20}$$

Here, $a_N\left(E_0,\theta_0\right)$ and $a_E\left(E_0,\theta_0\right)$ are the number and energy of albedos; and $a\left(E_0,\theta_0;E,\theta,\varphi\right)$ is the differential albedo, which is integrated over the energy domain dE as well as over the polar and azimuthal domains (dθ and dφ, respectively). For the Monte Carlo simulations, the total number and energy albedo are computed by replacing the integrals in Eqs. (21) and (22) with a finite sum and tallying for the particles in all directions and energies, which can be expressed as follows:

$$\alpha_N\left(E_0,\theta_0\right) = \frac{\sum_{i=1}^{N_R} w_i}{\varphi_0}, \tag{21}$$

$$\alpha_E\left(E_0,\theta_0\right) = \frac{\sum_{i=1}^{N_R} \frac{E_i}{E_0}.w_i}{\varphi_0}, \tag{22}$$

where w_i and E_i are the weight and energy of the ith particle, respectively; and E_0 is the incident energy. A schematic representation of the reflection process in the material is shown in Fig. 4.

3 EJUSCO code

The EJUSTCO code was written in MATLAB as a script file. The program begins by inputting the necessary data, followed by the computation of once and for all calculations, such as establishing the energy mesh, cross-sectional tables, and geometric boundaries, as well as initializing different counters for scoring. Subsequently, the program specifies the initial positions and directions of the photons. The cross-section is interpolated using the photon's initial energy, and the path length to the first collision is calculated. Next, the particle is shifted to the first collision site via translation, as expressed in Eq. 9. At the new position, the code interrogates the geometry to determine whether the photon crosses an internal boundary; if it does, then the energy and dose are scored in this region. If the crossing suggests that the photon is outside the medium, i.e., either at the front or back, then the photon history is terminated and a new photon history is started. If the photon remains in the medium, then it is shifted to the collision site. Because the photoelectric effect is not allowed directly, the type of interaction, whether Compton scattering or pair production, is determined by comparing a random number to the ratio of an individual interaction cross-section to the total cross-section.

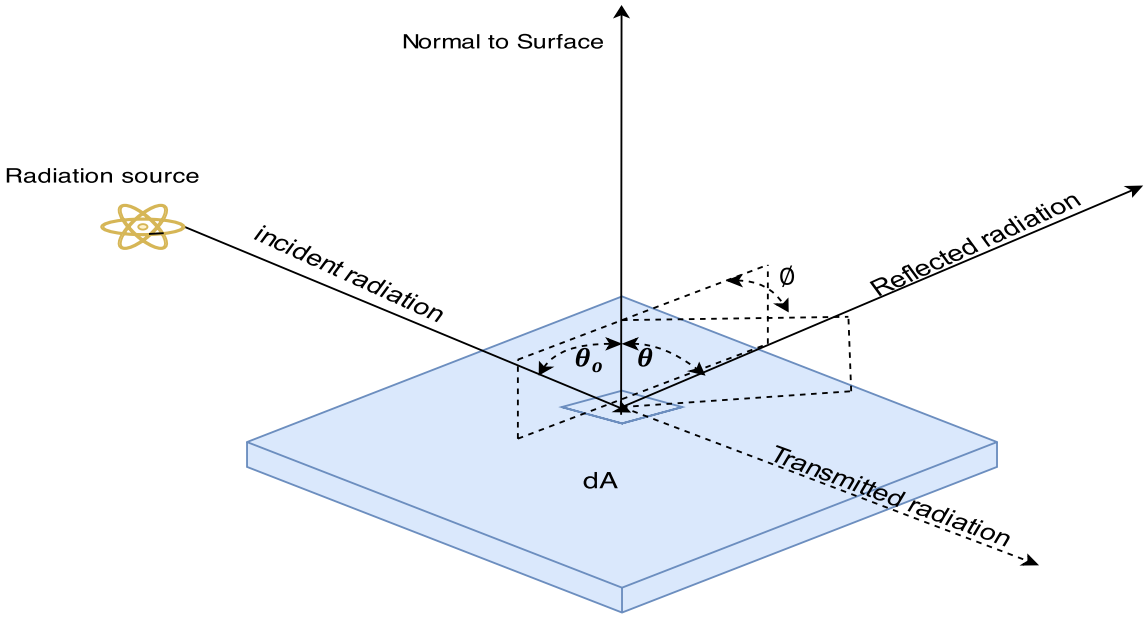

Fig. 4 Illustration showing gamma rays reflected from a surface. In most shielding applications, the interface between air and a shielding material is of interest, with the shield material being the reflective surface (adapted from [14])

If the interaction involves scattering, then the new photon energy is determined by the angle of scattering sampled from the Klein–Nishina distribution using the Khan or Koblinger method, depending on the initial photon energy. Subsequently, the photon directional cosines are determined using the rotational techniques described in Sect. 2.5. If pair production occurs, then an annihilated photon with energy 0.511 MeV is followed with a weight of 2. In either scattering or pair production, the photon is followed by repeating the process above until the photon departs from the medium, the energy falls below the energy cutoff, or the history is terminated in the Russian roulette. In double- and triple-layer systems, a routine is entered after a tentative path length is obtained to verify whether the particle has entered a new region of a different material. If it has, then the routine sets the distance to the boundary and calculates a new path length using the correct regional cross-section. A flow diagram of the programming algorithm is shown in Fig. 5.

4 Results and discussion

4.1 Comparison of EJUSTCO simulation with literature

The aim of this study is to develop a code to investigate gamma-ray transport through different shielding materials and calculate the quantities used to evaluate the capability of gamma-ray shields. In the initial study, monoenergetic photons with an energy of 0.662 MeV were simulated using 20,001 photons/cm^2/s as the number of histories in a lead medium with a thickness of 1.7 cm (two mean free paths). The photon distribution, deposited energy, and final positions of the photons after each cycle are shown in Fig. 6. This plot allows the particle behavior within a material to be visualized and understood easily.

The fates of the photons after the simulations as fractions of the normalized photon history are presented in Table 1. In addition, the dose rate and buildup factor at material thicknesses of 1, 1.5, and 2 mfp were computed (see Table 2). The results shown in both tables were compared with those in the literature, and the percentage errors were computed.

Figure 7 shows the energy spectrum of gamma rays transmitted onto the surface of a 2-mfp-thick water medium, which agreed well with that obtained from the wood MONTERAY Mark (I) code.

In another simulation using the same number of particle histories, the effect of pair production inclusion on the fate of photons, buildup factor, and dose rate was investigated using lead with thicknesses of 1 and 3 mfp and a monoenergetic photon source of 10 MeV. The results without pair production are presented in Tables 3 and 4, whereas those with pair production are presented in Tables 5 and 6. In both cases, the results were compared with those reported in the literature. The results of this study show that at energies above 1.022 MeV, the effect of pair production is not negligible as it increases the buildup factor and hence the number of absorption processes in the media. The EJUSTCO

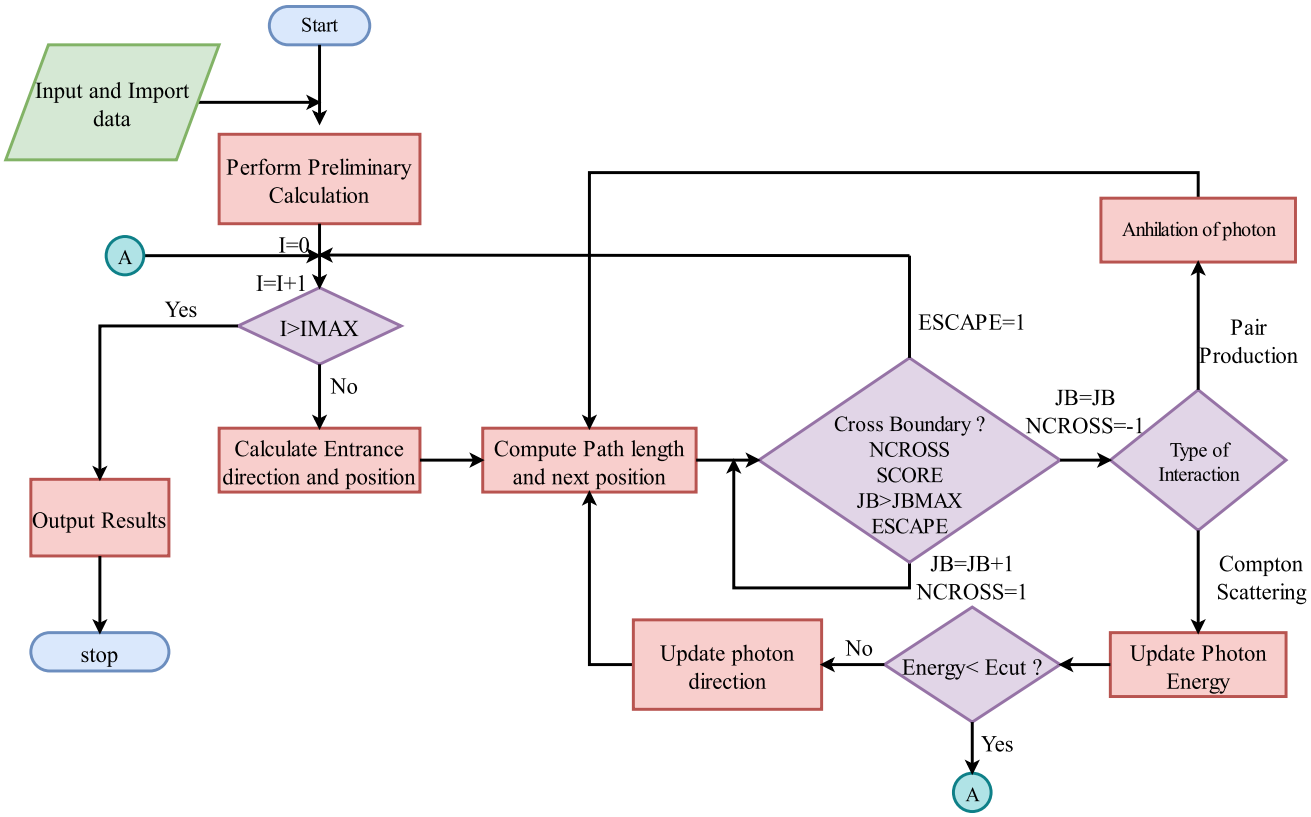

Fig. 5 Flow chart of EJUSTCO algorithm

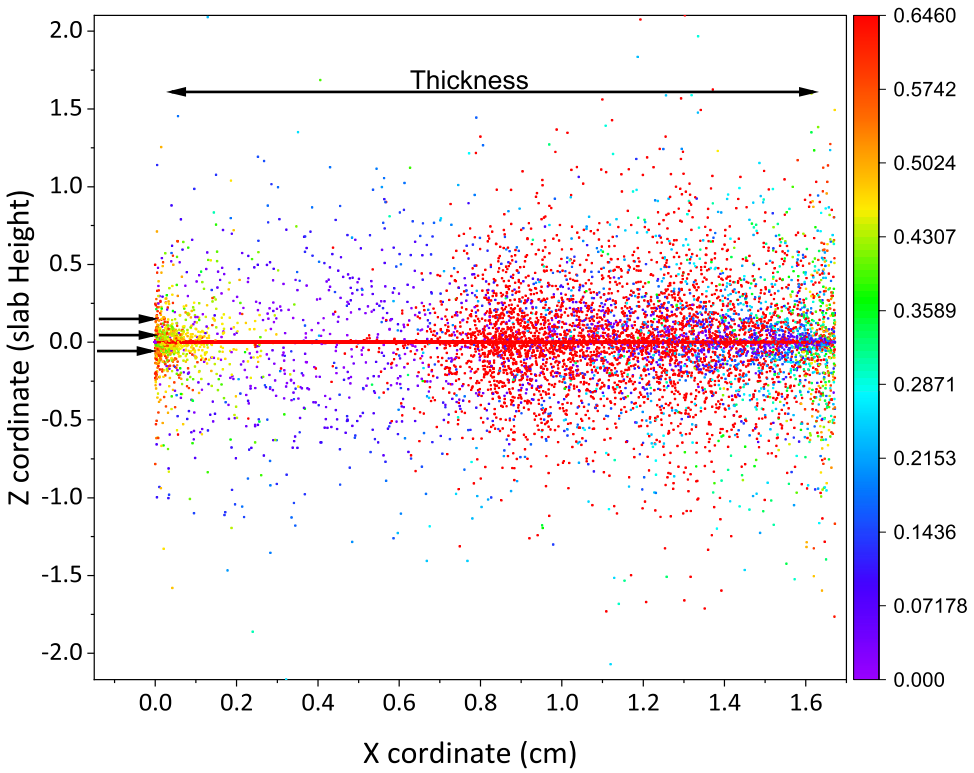

Fig. 6 (Color online) Distribution of final position of each photon after each history in lead media using EJUSTCO

Table 1 Photon fate (total fraction = 1) without pair production inclusion at 6 MeV in water

Photons fate	EJUSTCO	Wood [13]	Error (%) = $\frac{\lvert EJUSTCO-WOOD\rvert}{WOOD}$
Absorbed in medium	0.23	0.2315	0.647948
Photons transmitted through medium	0.6698	0.6707	0.134188
Photons reflected from medium surface	0.1001	0.0978	2.351738
Photons with $E < E_{cut}$	3.59E-06	3.82E-06	6.020942

Table 2 Dose rate and exposure buildup factor comparison at 6 MeV in water

Thickness (mfp)	Parameters	EJUSTCO	Wood	Error (%) = $\frac{\lvert EJUSTCO-WOOD\rvert}{WOOD}$
1	Dose rate (R/hr)	0.062	0.0622	0.321543
	Exposure Buildup factor	1.406	1.413	0.4954
1.5	Dose rate (R/hr)	0.0428	0.0428	0
	Exposure Buildup factor	1.6005	1.602	0.093633
2	Dose rate (R/hr)	0.0292	0.0292	0
	Exposure Buildup factor	1.7993	1.802	0.149834

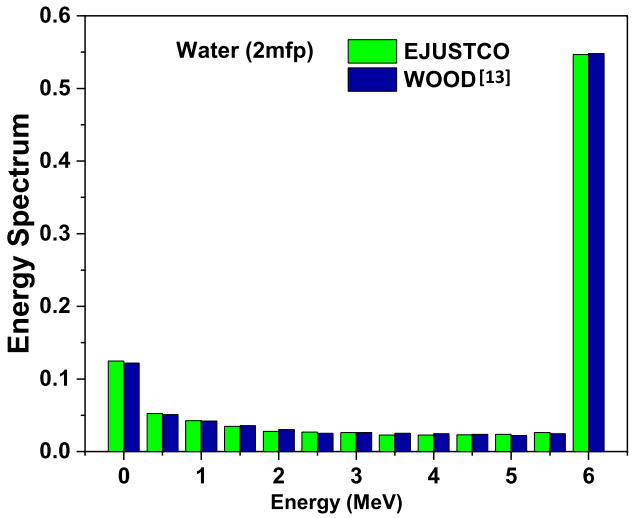

Fig. 7 (Color online) Energy spectrum of gamma-ray (6 MeV) transmitted to 2-mfp-thick water

simulation results agreed well to the results from literature for both cases. The energy spectrum for the case of 3-mfp-thick lead is presented in Fig. 8 for comparison.

According to the literature, annihilated photons can be treated via two approaches, as explained in Sect. 2.1. Thus, to understand the effect of each model on the simulation results and computational time, both models were tested. Their effects are listed in Tables 7 and 8. As shown in Table 7, the simple model can be safely employed because its figure-of-merit (FOM) is higher than that of the classical model, thus confirming the assertions presented in the literature. Meanwhile, Table 8 shows that employing a simple model significantly reduces the computational time by more than one-half of that required by the classical model. Therefore, all other analyses were performed using a simple model.

4.2 Comparison of exposure buildup factor results in single materials with standard codes and data

To fully ascertain the usefulness and robustness of the code, it must be validated by comparing the results yielded by it with standard codes and data for different materials with varying thicknesses and photon energies. Thus, exposure buildup factors computed using the EJUSTCO code were validated for water (Table 9), lead (Table 10), iron (Table 11), aluminum (Table 12), and concrete (Table 13) based on results obtained from the EGS4 [29] and MCNP [30] standard codes and the ANS-6.4.3 standard [31] for material thicknesses up to 8 mfp and energies of 1, 2, 3, and 4 MeV. In all cases, a particle history of 1×10^6 was used

Table 3 Photon fate (total fraction = 1) without pair production inclusion at 10 MeV in lead

Photons fate	EJUSTCO	Wood	Error (%) = $\frac{\lvert EJUSTCO-WOOD\rvert}{WOOD}$
Absorbed in medium	0.5521	0.5529	0.144692
Photons transmitted through medium	0.4442	0.4438	0.090131
Photons reflected from medium surface	0.0035	0.0033	6.060606
Photons with $E < E_{cut}$	1.36E-27	1.09E-27	24.77706

Table 4 Comparison of contributions of dose rate and exposure buildup factor without pair production at 10 MeV in lead

Thickness (mfp)	Parameters	EJUSTCO	Wood	Error (%) = $\frac{\lvert EJUSTCO-WOOD\rvert}{WOOD}$
1	Dose rate (R/hr)	0.0777	0.0738	5.284553
	Exposure Buildup factor	1.1	1.1	0
3	Dose rate (R/hr)	0.012	0.012	0
	Exposure Buildup factor	1.42	1.41	0.70922

Table 5 Photon fate (total fraction = 1) with pair production inclusion at 10 MeV in lead

Photons fate	EJUSTCO Pair frac. = 0.4812	Wood Pair frac. = 0.4893	Error (%) = $\frac{\lvert EJUSTCO-WOOD\rvert}{WOOD}$
Absorbed in medium	0.6239	0.6707	1.580438
Photons transmitted through medium	0.3240	0.2648	22.35695
Photons reflected from medium surface	0.0559	0.0645	13.33333
Photons with $E < E_{cut}$	8.88E-26	8.80E-26	0.852273

Table 6 Comparison of contributions of dose rate and exposure buildup factor with pair production at 10 MeV in lead

Thickness (mfp)	Parameters	EJUSTCO	Wood	Error (%) = $\frac{\lvert EJUSTCO-WOOD\rvert}{WOOD}$
1	Dose rate (R/hr)	0.075	0.0759	1.185771
	Exposure Buildup factor	1.13	1.14	0.877193
3	Dose rate (R/hr)	0.0125	0.0126	0.793651
	Exposure Buildup factor	1.4	1.41	0.70922

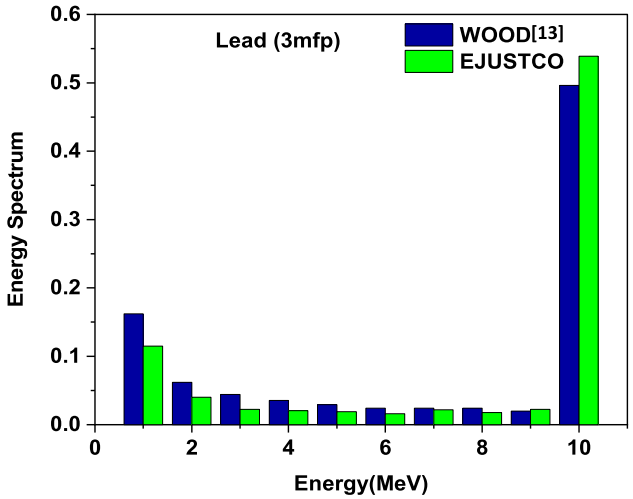

Fig. 8 (Color online) Energy spectrum of gamma-ray (10 MeV) transport in 3-mfp-thick lead

in the validation, which resulted in an average maximum standard error of approximately 5%.

4.3 Exponential transform parameter prediction using ANN

As stated in Sect. 2, determining an arbitrary parameter for use in the simulation when the exponential transformation technique is active can be time consuming and may require several trials. Therefore, some knowledge regarding the expected value is required. Hence, an ANN model was trained to predict these parameters. The model was trained using the Levenberg–Marquardt algorithm, which achieved an MSE of 0.00076752, as shown in Figs. 9, 10 shows the regression plots of the training and validation data. In the regression, the accuracy of data fitting for training was indicated by an *R*-value of 0.99527.

The error and fitting accuracy confirmed that the model can be used to predict the parameter c. The values predicted using the ANN model were compared with those obtained using the EJUSTCO code (see Table 14). The results confirmed the viability of using ANNs to predict the exponential transform parameter. However, because of the few data points employed, predictions beyond the range of the dataset would be inaccurate, which is a significant disadvantage in employing ANNs in regression analysis. Hence, increasing the dataset would extend its applicability beyond current data ranges. To demonstrate the representativeness of the

Table 7 Efficiency of pair production strategy on dose rate and buildup factor calculation

Thickness (mfp)	Parameters	Simple model	Classical model	FOM simple model	FOM classical model
1	Dose rate (R/hr)	0.075	0.075	8008.9	2541.02
	Exposure Buildup factor	1.135	1.142	97	30.99
3	Dose rate (R/hr)	0.0134	0.0132	31,087.8	10,331.70
	Exposure Buildup factor	1.49	1.48	7.016	2.328

Table 8 Effect of pair production strategy on computational time

Computational time for simple model (s)	Computational time for classical model (s)
123.28	389.6

training dataset, Fig. 11 shows the distribution of the data in terms of the input parameters. Figure 11a shows that the energy range extends from low to high energies in a range between 0.5 and 10 MeV. Similarly, Fig. 11b shows the distribution of the densities used in the training. Based on the distribution, the density spans from less dense to highly dense materials, thus capturing materials of diverse densities. Further analyses were conducted to understand the effect of incorporating the ANN model on the computational time required by EJUSTCO. The computational times required when the ANN model was used and not used were 88.776 and 89.673 s, respectively, based on a photon history of 20,000. Clearly, incorporating the ANN model did not significantly affect the EJUSTCO code.

In Table 15, the total times required to predict parameter C using trial and error and the ANN model are listed. Using trial and error, an average of four trials was required, which corresponded to a total time of 1287.44 s. However, no trials were necessitated for the ANN and hence a short time of 273.47 s was required. The results clearly indicate that the ANN is advantageous because it does not require simulation trials to determine the optimum value. Additionally, the effect of the ANN inclusion on the efficiency of the simulation must be ascertained. Thus, the FOMs of different simulation trials involving aluminum, lead, and carbon at 3 MeV were computed (see Table 16). For the simulation involving aluminum and lead, the FOMs were extremely high in the simulation employing the ANN compared with that without the ANN. However, the FOM for the carbon simulation with the ANN was lower than that without the ANN. This shows that incorporating the ANN can significantly affect the simulation efficiency, which is primarily governed by the prediction accuracy, as listed in Table 14.

Table 9 Comparison of exposure buildup factor in water, where standard error between EJUSTCO and other standard results is shown

Energy (MeV)	mfp	Water			Error (%) $= \frac{\lvert EJUSTCO - ANS - 6.4.3\rvert}{ANS - 6.4.3}$	Error (%) $= \frac{\lvert EJUSTCO - EGS4\rvert}{EGS4}$
		EJUSTCO	ANS-6.4.3	EGS4		
1	1	1.87	2.08	2.04	9.97	8.21
	2	2.99	3.62	3.57	17.30	16.14
	3	4.44	5.5	5.54	19.33	19.92
	4	6.23	7.68	7.75	18.84	19.57
	5	9.00	10.1	10.2	10.93	11.81
	6	11.88	12.8	12.9	7.18	7.89
	7	14.98	15.8	15.9	5.17	5.77
	8	19.74	19	19.2	3.91	2.83
3	1	1.65	1.71	1.66	3.48	0.58
	2	2.35	2.46	2.41	4.63	2.66
	3	3.11	3.23	3.23	3.75	3.75
	4	3.95	4	4.03	1.23	1.96
	5	4.74	4.8	4.83	1.17	1.78
	6	6.53	5.61	5.63	16.43	16.02
	7	7.70	6.43	6.5	19.72	18.43
	8	8.14	7.27	7.4	11.99	10.02

Table 10 Comparison of exposure build up factor in lead, where standard error between EJUSTCO and other standard results is shown

Energy (MeV)	mfp	Lead			Error (%) = $\frac{\lvert EJUSTCO-ANS-6.4.3\rvert}{ANS-6.4.3}$	Error (%) = $\frac{\lvert EJUSTCO-EGS4\rvert}{EGS4}$
		EJUSTCO	ANS-6.4.3	EGS4		
1	1	1.36	1.31	1.36	3.73	0.08
	2	1.61	1.61	1.69	0.24	4.51
	3	1.89	1.87	1.92	0.94	1.69
	4	2.06	2.1	2.18	1.71	5.32
	5	2.45	2.32	2.42	5.81	1.44
	6	2.66	2.54	2.66	4.89	0.16
	7	2.46	2.75	2.88	10.37	14.41
	8	2.56	2.96	3.05	13.59	16.14
3	1	1.35	1.41	1.43	4.17	5.51
	2	1.65	1.77	1.71	6.74	3.47
	3	1.98	2.13	2.13	7.16	7.16
	4	2.35	2.51	2.51	6.38	6.38
	5	2.70	2.91	2.94	7.19	8.13
	6	3.21	3.34	3.39	3.93	5.35
	7	3.83	3.81	3.87	0.43	1.12
	8	4.42	4.3	4.43	2.83	0.19

Table 11 Comparison of exposure build up factor in iron, where standard error between EJUSTCO and other standard results is shown

Energy (MeV)	mfp	Iron			Error (%) = $\frac{\lvert EJUSTCO-ANS-6.4.3\rvert}{ANS-6.4.3}$	Error (%) = $\frac{\lvert EJUSTCO-EGS4\rvert}{EGS4}$
		EJUSTCO	ANS-6.4.3	EGS4		
1	1	1.78	1.85	1.76	4.04	0.87
	2	2.61	2.85	2.83	8.25	7.61
	3	3.66	4	4.03	8.39	9.08
	4	5.01	5.3	5.3	5.56	5.56
	5	6.25	6.74	6.77	7.33	7.74
	6	8.03	8.31	8.38	3.43	4.23
	7	9.64	10	10.1	3.62	4.57
	8	12.44	11.8	12	5.41	3.65
3	1	1.57	1.64	1.64	4.04	4.04
	2	2.20	2.28	2.24	3.47	1.74
	3	2.85	2.96	3.01	3.75	5.35
	4	3.54	3.68	3.71	3.94	4.71
	5	4.29	4.45	4.49	3.62	4.48
	6	4.78	5.25	5.31	8.98	10.01
	7	5.69	6.09	6.16	6.61	7.67
	8	6.79	6.96	7.02	2.50	3.34

4.4 Dose rate analysis in single- and triple-layer material systems

This section presents the dose rate calculated using the EJUSTCO code for single- and triple-layer systems. The dose rates in aluminum, lead, water, concrete, and iron are shown in Fig. 12 for the 1 and 3 MeV energy sources. As shown in the plot, the dose reduction reflects an exponential decay, which characterizes gamma-ray attenuation. Furthermore, the attenuation reduction for both energies shows that

Table 12 Comparison of exposure build up factor in aluminum, where standard error between EJUSTCO and other standard results is shown

Aluminium				
Energy (MeV)	Thickness (mfp)	EJUSTCO	ANS-6.4.3	Error (%) = $\frac{\lvert EJUSTCO-ANS-6.4.3\rvert}{ANS-6.4.3}$
1	1	2.02	1.99	1.51
	2	3.26	3.26	0.00
	4	6.37	6.48	1.70
3	1	1.68	1.68	0.00
	2	2.38	2.38	0.00
	4	3.92	3.86	1.55

Table 13 Comparison of exposure build up factor in concrete, where statistical error between EJUSTCO and other standard results is shown

Energy (MeV)	Thickness (mfp)	Concrete		Error (%) = $\frac{\lvert EJUSTCO-MCNP\rvert}{MCNP}$
		EJUSTCO	MCNP	
1	1	2.05	2.05	0.00
	2	3.34	3.31	0.91
	3	4.76	4.88	2.46
	4	6.51	6.59	1.21
	5	8.9	8.54	4.22
	6	11.29	10.22	10.47
	7	14.7	12.18	20.69
	8	16.26	15.46	5.17
2	1	1.86	1.86	0.00
	2	2.85	2.83	0.71
	3	3.96	3.72	6.45
	4	5.08	4.77	6.50
	5	6.44	5.81	10.84
	6	7.63	7.12	7.16
	7	8.96	8.24	8.74
	8	9.19	9.36	1.82
4	1	1.59	1.77	10.17
	2	2.18	2.23	2.24
	3	2.81	3.01	6.64
	4	3.45	3.45	0.00
	5	4.16	4.16	0.00
	6	4.86	4.88	0.41
	7	5.72	5.56	2.88
	8	6.18	6.11	1.15

as the energy increases, the ability of the materials to shield gamma rays decreases owing to the decrease in the attenuation coefficient of the material.

Similarly, the dose rates within layered materials are shown in Figs. 13 and 14, which have been validated via comparison with results in the literature [14, 32]. Based on the figures, the behavior of photon attenuation can be visualized, i.e., the attenuation process involves a combination of individual materials within the system. To demonstrate the attenuation performance of different single materials and their combinations in triple-layer systems, the efficiencies of these systems were computed, as shown in Fig. 15.

4.5 Comparison of exposure buildup factor in double layer system with standard codes and data

The transmission buildup factors for double-layer systems were investigated. Specifically, the buildup factor values for an iron–water system (medium- and high-atomic-number

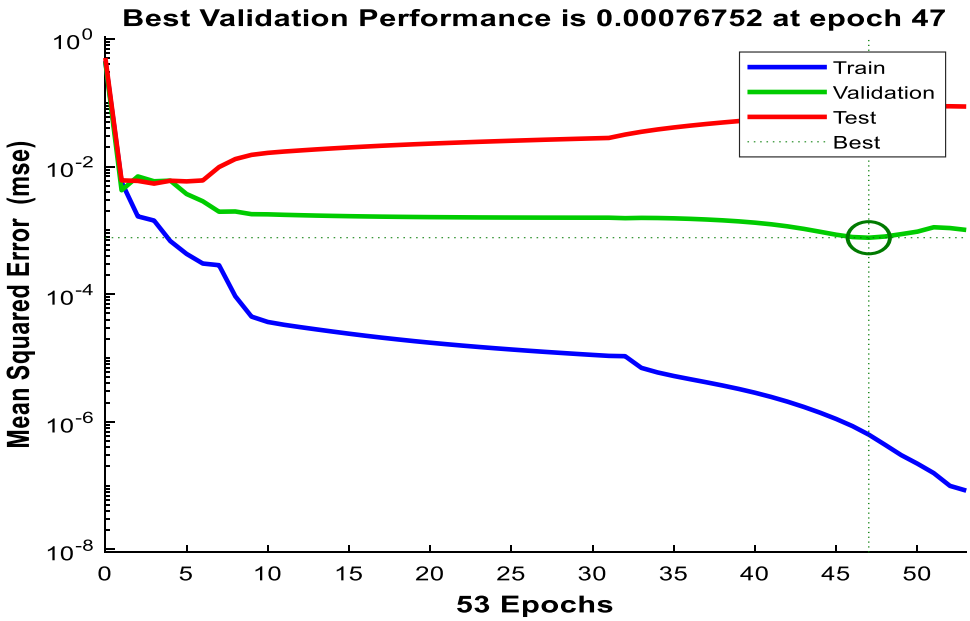

Fig. 9 (Color online) Mean square error analysis of ANN training

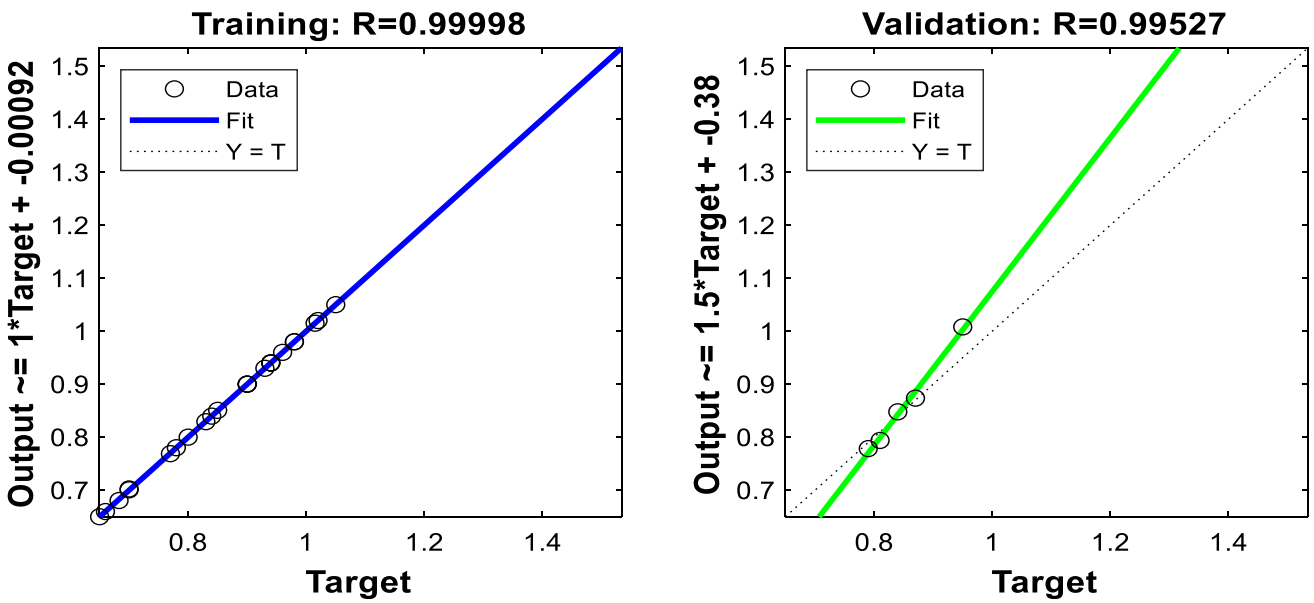

Fig. 10 Regression plots showing fitting performance of the ANN model

materials) were investigated for two cases. In the first case (as presented in Table 17), the iron thickness fixed while the thickness of water was varied at energies of 1 and 3 MeV. Meanwhile, the converse was applied for the second case, as shown in Table 18. The results from both cases were compared with the results yielded by the EGS4 and MCBLD codes in the literature. Finally, the transmission buildup factors for double layers of lead, aluminum, and iron were validated at energies of 0.662 and 1.25 MeV via comparison with experimental results. In all cases, the results showed good agreement, as presented in Table. 19. The exposure buildup factor of the triple-layer materials was computed and compared with the results yielded by the EGS and PENELOPE codes and an empirical formula derived by Lin and Jiang [29] (see Table 20).

4.6 Total number and energy albedo computation using EJUSTCO for perpendicular incidence

The concept of albedo is provided in the Introduction section and in Sect. 2. This section presents the numerical results obtained via EJUSTCO simulations. Figures 16 and 17 show

Table 14 Comparison of parameter c predicted by ANN model with data observed from EJUSTCO code

Material	Energy	EJUSTCO	ANN	Error (%) = $\frac{\lvert ANN-EJUSTCO \rvert}{EJUSTCO}$
Aluminum	0.5	0.77	0.77	0
	0.8	0.83	0.83	0
	3	0.94	0.94	0
	6	0.96	0.96	0
Lead	0.5	1.023	1.02	0
	0.8	1.015	1.02	0
	3	0.93	0.93	0
	6	0.9	0.90	0
Carbon	0.5	0.69	0.76	0.1
	0.8	0.73	0.77	0.05
	3	0.92	0.60	0.34
	6	0.98	0.87	0.11

Table 15 Total computational time to predict parameter C using trial and error and the ANN model

Mechanism	Average number of trials	Total computational time (s)
Trial and Error	4	1287.445
ANN	Not applicable	273.471

Table 16 Effect of the incorporating the ANN model on simulation efficiency

Material	EJUSTCO FOM	EJUSTCO/ANN FOM
Aluminium	0.575	0.661
Lead	0.6046	0.611
Carbon	0.464	0.277

the total number albedo values for aluminum and water at varying energies. The results were validated using the Monte Carlo codes MCNP, FOTELP, and PENELOPE. As shown in the figures, all the codes agreed well with one another, thus indicating the ability of the developed code to accurately compute albedo values. The general trend shows that the albedo increases with energy and is lower for heavier materials because of the increased absorption rate in such materials. These observations are consistent with those reported previously.

Similarly, Fig. 18 shows the energy albedo for both water and aluminum, where the same trend is shown. However, a slight error exists between our code and that of MCNP, which is attributable to the nonconsideration of coherent scattering and secondary photon emissions [33] in our code. Nonetheless, the results show good agreement.

5 Conclusions and future directions

Motivated by the demand for a Monte Carlo code that can be easily accessed without constraints for radiation shielding analysis, we developed EJUSTCO using the Monte Carlo technique. In this study, the code was employed to evaluate the shielding performance and parameters of radiation-shielding materials. The code simulates gamma-ray particles through different material media by considering the primary interaction mechanisms, such as Compton scattering, the photoelectric effect, pair production, and gamma ray annihilation. The EJUSTCO code adopts a non-analog Monte Carlo approach using survival weight, the Russian roulette, and exponential transform techniques to improve computational efficiency. The parameters for the exponential transform were predicted based on data

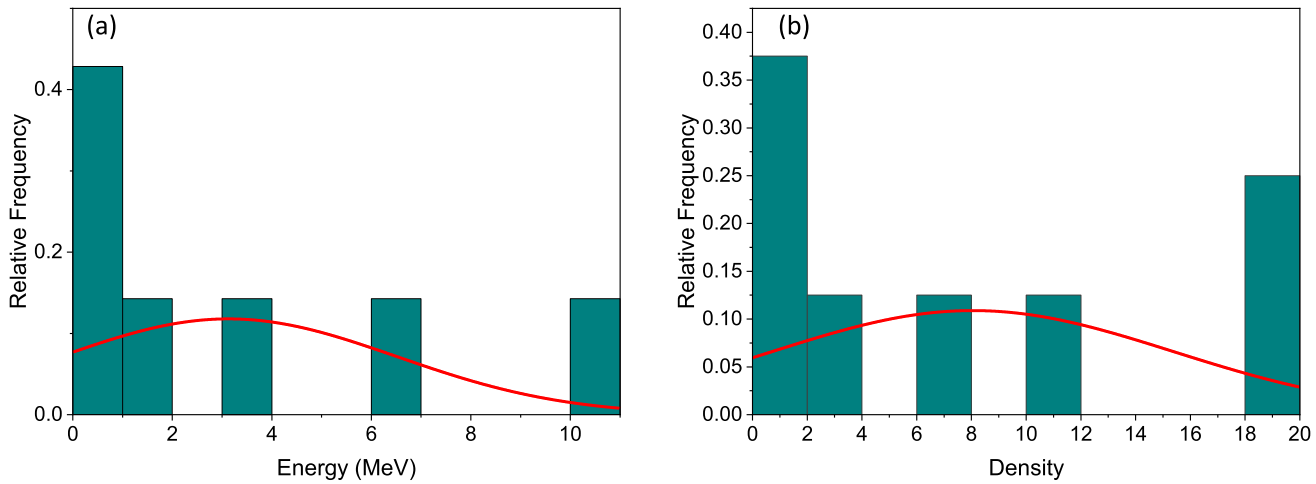

Fig. 11 Distribution of training sample based on input parameters

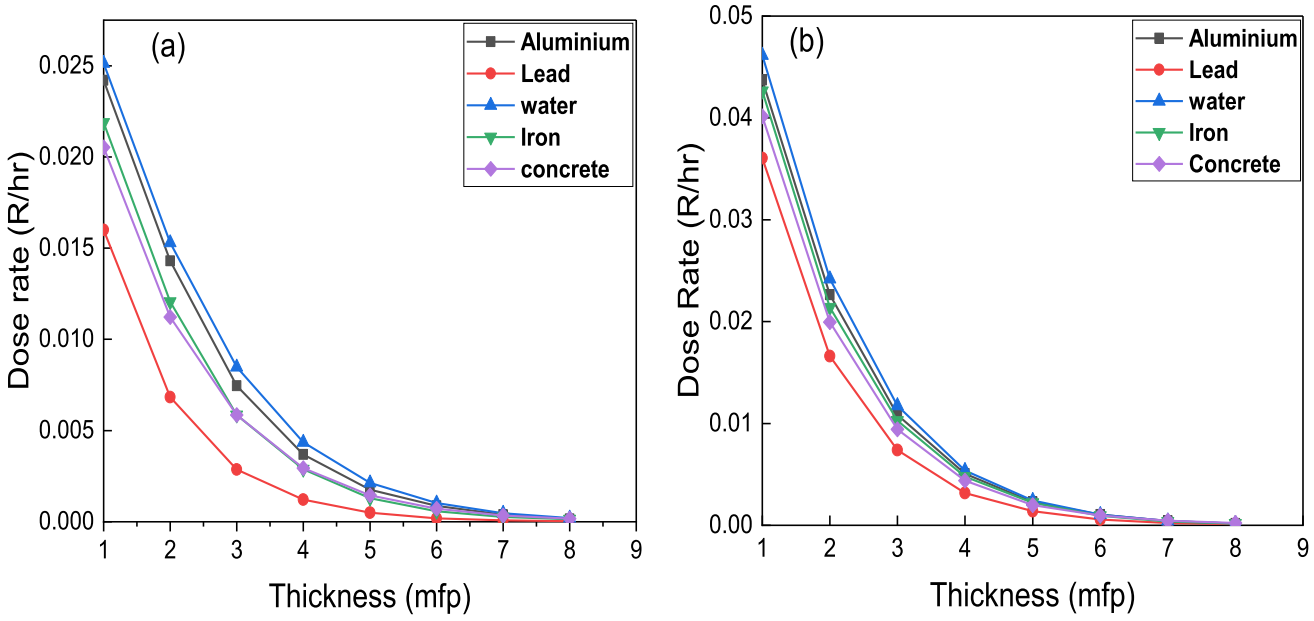

Fig. 12 (Color online) Dose rate for iron, lead, and water at 1 MeV (**a**) and 3 MeV (**b**) with 8 mfp thickness, as predicted by EJUSTCO

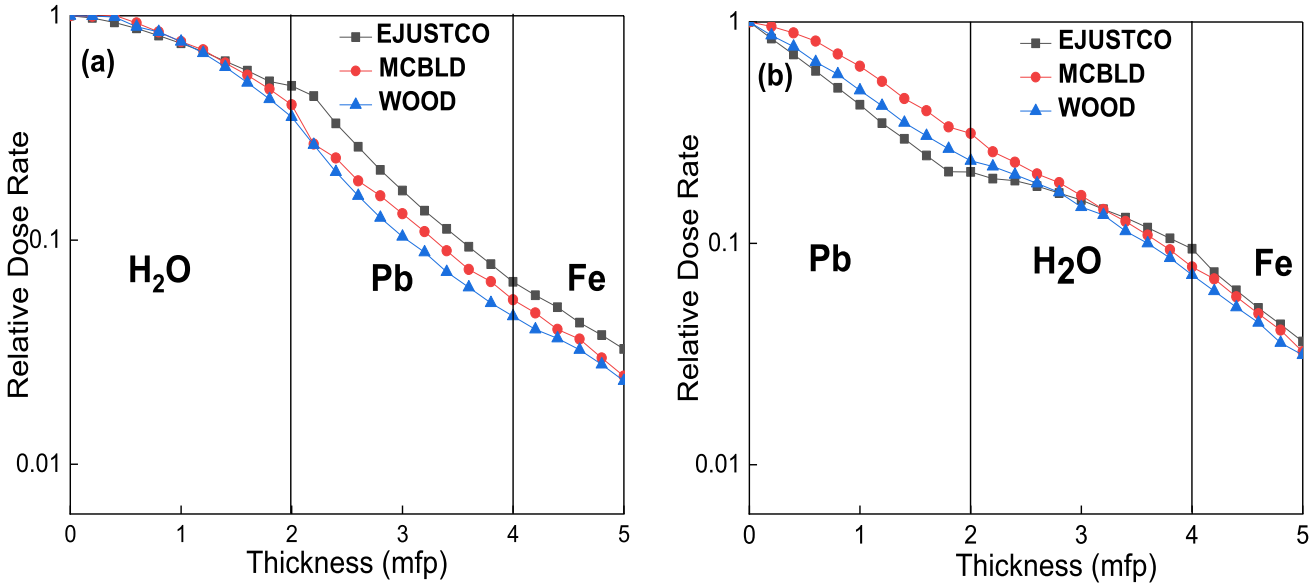

Fig. 13 EJUSTCO prediction of relative dose rate variation for different triple-layer shield systems: **a** water/lead/iron and **b** lead/water/iron for 1 MeV gamma photon

obtained through trial and error. The model achieved an MSE of 0.00076752 and an R-value of 0.99998, which demonstrated the viability of the model. The model eliminates the necessity for such trials when a simulation is to be performed, provided that the required value involves inputs within the range of data used in to train the model. Thus, generalizability beyond the data points is not guaranteed. Based on this limitation, the dataset should be extended to increase the generalization of the model. The exposure buildup factor and dose rate values in single-, double-, and triple-layer materials of lead, iron, concrete, aluminum, and water were investigated. The exposure buildup values were validated with results yielded by MCNP, EGS4, ANS-6.4., MCBLD, and MONTEREY codes. The EJUSTCO code performed well, achieving average values of 5.6% for the exposure buildup factor in single materials, 2.75% in double-layer materials, and 10% in triple-layer materials. However,

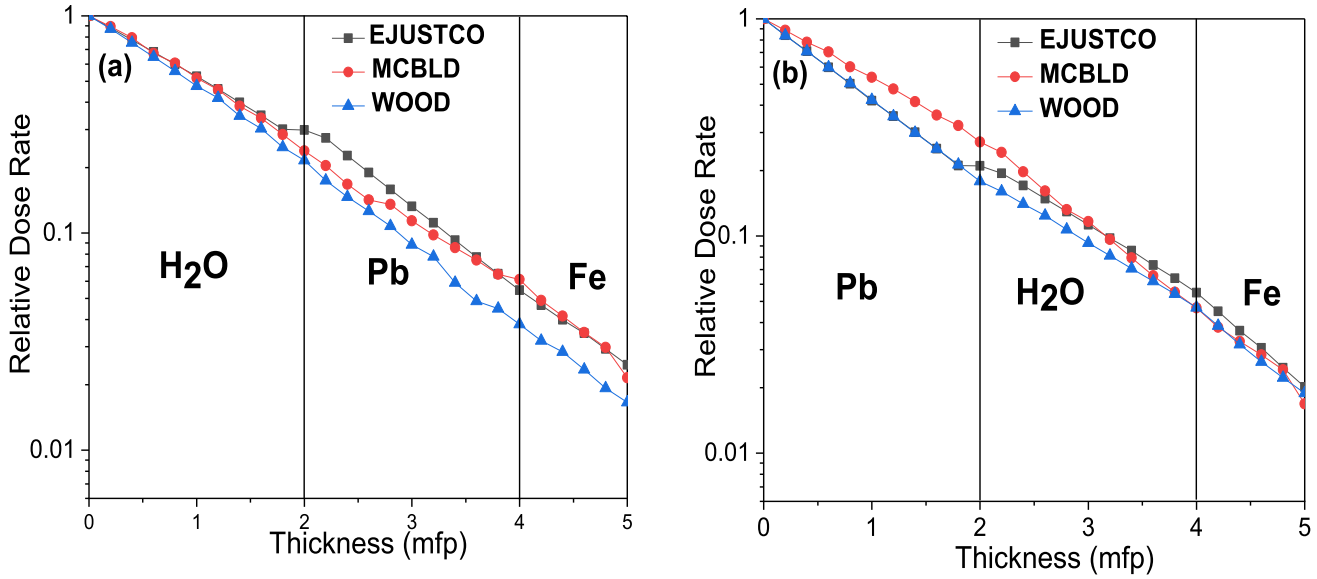

Fig. 14 EJUSTCO prediction of relative dose rate variation for different triple-layer shield systems: **a** water/lead/iron and **b** lead/water/iron for 10 MeV gamma photon

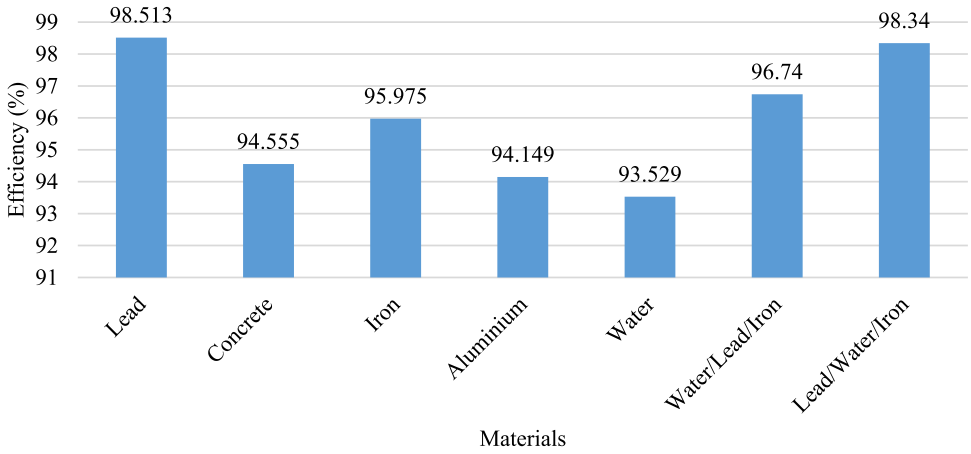

Fig. 15 Efficiencies of single and triple-layer materials with 5 mfp thickness in attenuating gamma radiation, as predicted by EJUSTCO

Table 17 Comparison of transmission double-layer exposure buildup factor in iron/ water system

Energy (MeV)	Media/Thickness (mfp)	EGS4	EJUSTCO	Error (%) = $\frac{\lvert EJUSTCO-EGS4\rvert}{EGS4}$
1	$2Fe+1H_2O$	4.23	4.7	11.11
	$2Fe+2H_2O$	6.37	6.51	2.20
	$2Fe+3H_2O$	8.73	8.52	2.41
	$2Fe+4H_2O$	10.4	10.25	1.44
	$2Fe+5H_2O$	13.7	13.05	4.74
	$2Fe+6H_2O$	16.4	17.14	4.51
3	$2Fe+1H_2O$	2.96	2.94	0.68
	$2Fe+2H_2O$	3.74	3.52	5.88
	$2Fe+3H_2O$	4.45	4.25	4.49
	$2Fe+4H_2O$	5.19	4.99	3.85
	$2Fe+5H_2O$	5.97	6.38	6.87
	$2Fe+6H_2O$	6.58	6.82	3.65

Table 19 Comparison of transmission double-layer exposure buildup factor for different configurations of lead, iron, and aluminum

Energy(MeV)	Media/Thickness (cm)	EJUSTCO	EXP	Error (%) = $\frac{\lvert EJUSTCO-EXP\rvert}{EXP}$
0.662	2Al–2Pb	1.46	1.46	0.00
	2Pb–2Al	1.409	1.408	0.07
	2Fe–2Al	1.46	1.49	2.01
	2Al–2Fe	1.59	1.55	2.58
	2Pb–2 Fe	2.08	2.08	0.00
	2Fe–2Pb	1.85	1.85	0.00
1.25	2Al–2Pb	1.72	1.73	0.58
	2Pb–2Al	1.66	1.67	0.60
	2Fe–2Al	1.36	1.38	1.45
	2Al–2 Fe	1.45	1.45	0.00
	2Pb–2Fe	2.02	2.03	0.49
	2Fe–2Pb	1.76	1.76	0.00

Table 18 Comparison of transmission double layer exposure buildup Factor in water/ iron system

Energy (MeV)	Media/Thickness (mfp)	EGS4	EJUSTCO	Error (%) = $\frac{\lvert EJUSTCO-EGS4\rvert}{EGS4}$
1	$2H_2O+1Fe$	3.78	3.59	5.03
	$2H_2O+2Fe$	4.71	4.64	1.49
	$2H_2O+3Fe$	5.83	6.06	3.95
	$2H_2O+4Fe$	6.9	7.4	7.25
	$2H_2O+5Fe$	8.09	7.95	1.73
	$2H_2O+6Fe$	9.55	10.1	5.76
3	$2H_2O+1Fe$	2.89	2.97	2.77
	$2H_2O+2Fe$	3.48	3.52	1.15
	$2H_2O+3Fe$	4.13	4.01	2.91
	$2H_2O+4Fe$	4.82	4.72	2.07
	$2H_2O+5Fe$	5.52	5.74	3.99
	$2H_2O+6Fe$	6.19	6.28	1.45

this errors are anticipated because the coherent scattering was not considered. However, for the energy values used in the computation, the coherent scattering event is negligible because the photon trajectory reaches a peak at such energies. The dose rate behavior in the single- and triple-layer materials was investigated, and the profile corresponded to that reported in the literature. The shielding efficiency when using a single- or triple-layer shield was demonstrated by analyzing the attenuation efficiencies in each system. The results showed that combining different materials with smaller thicknesses and consequently lower weights yielded the same attenuation of 98%, whereas a single material would require the same thickness with a higher weight. This finding is essential in cases where

Table 20 Comparison of transmission triple-layer exposure buildup factor for different configurations of lead, iron, and water

Energy (MeV)	Media/Thickness (mfp)	EGS	PENELOPE	Lin & Jiang	EJUSTCO	Error (%) = $\frac{\lvert EJUSTCO-EGS\rvert}{EGS}$	Error (%) = $\frac{\lvert EJUSTCO-Lin\rvert}{lin}$	Error (%) = $\frac{\lvert EJUSTCO-PENELOPE\rvert}{PENELOPE}$
1	$2H_2O+2Fe+1H_2O$	6.55		7.06	7.76	18.47	9.92	
	$2H_2O+2Fe+2H_2O$	8.82		9.81	9.61	8.96	2.04	
	$2Fe+2H_2O+1Fe$	6.91		6.63	6.78	1.88	2.26	
	$2Fe+2H_2O+2Fe$	8.07		7.74	7.8	3.35	0.78	
	$1Pb+1Fe+1H_2O$		2.7		3.77			39.62963
	$1Pb+1Fe+2H_2O$		4.39		4.47			1.822323

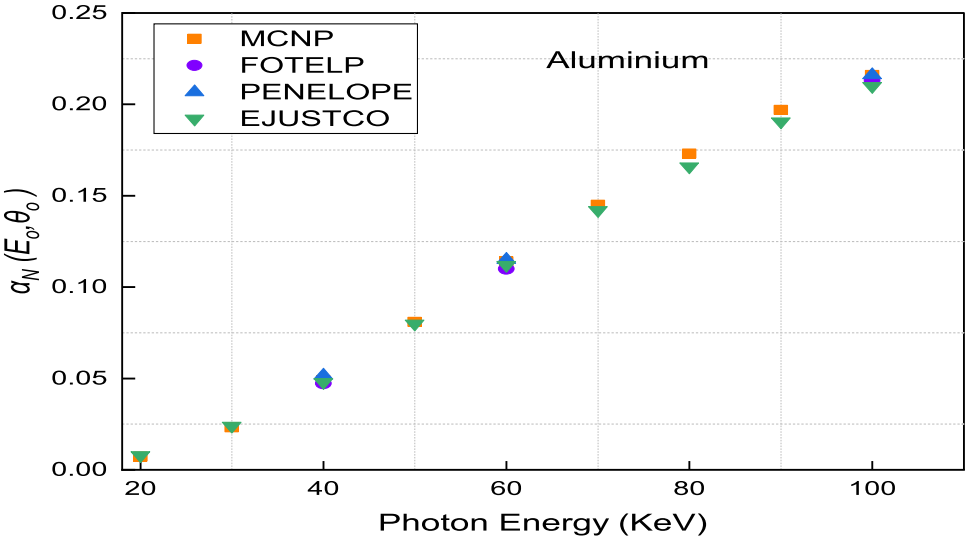

Fig. 16 Comparison of total number albedo as a function of energy computed using EJUSTCO with general purpose codes MCNP, FOTELP, and PENELOPE for aluminum

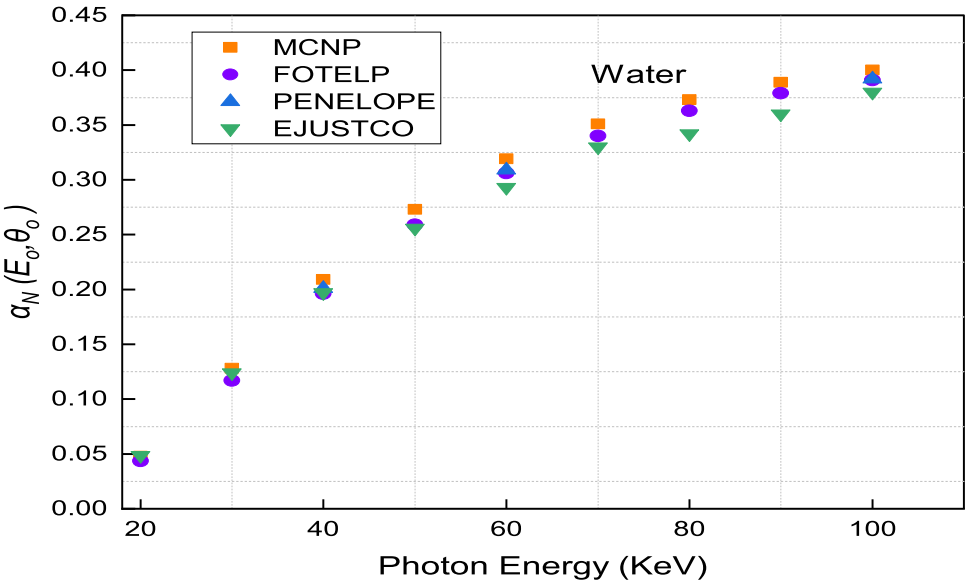

Fig. 17 Comparison of total number albedo as a function of energy computed using EJUSTCO with general purpose codes MCNP, FOTELP, and PENELOPE for water

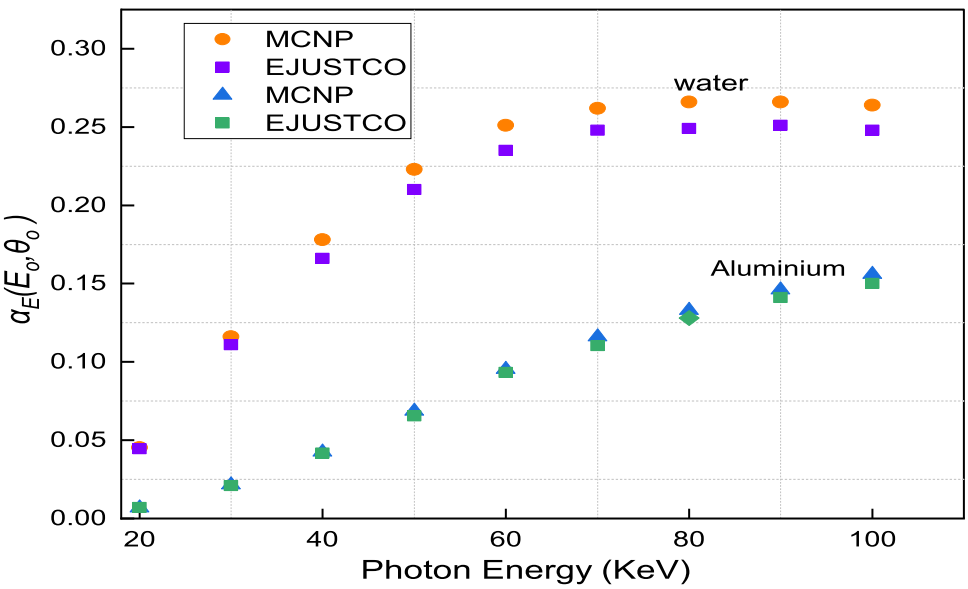

Fig. 18 Comparison of total energy albedo values computed using EJUSTCO and general-purpose code MCNP

the shield weight is significant, such as the transportation of radiation containers and shields used in the aerospace industry. Furthermore, the albedo is an important parameter in radiation shielding, particularly in areas where the radiation shield is exposed to radiation from a streaming duct. The albedo parameters computed in this study were the total number and energy albedos for aluminum and water. The values obtained during the simulation were compared with those yielded by MCNP, PENELOPE, and FOTELP. However, errors were observed in the total energy albedo values at high energies for water. This error was due to the nonconsideration of the coherent scattering mechanism and secondary photons, which are X-rays and bremsstrahlung gamma rays. The evidence for this assertion is based on the study conducted by Ezathola, which showed that these secondary photons contributed significantly to the albedo values, which implies that disregarding them affects the computed results. Additionally, coherent scattering becomes important for albedo values at high energies, and not considering it can result in a maximum error of 12%. Further studies should be performed by considering coherent events and simulating secondary photons. In conclusion, based on the results obtained thus far, the developed code performed satisfactorily. In future studies, a radiation source geometry other than the plane source considered in this study should be considered. Material geometries, such as spheres, cylinders, and other quadric geometries, should be considered as well. A geometry package based on combinatorial modeling or constructive solid geometrical modeling would be developed to allow the visualization of the radiation profile in the shielding material. The ANN dataset should be increased to extend its applicability to other points outside the current range. In addition, the applicability of employing a neural network to predict the cross-section using the Monte Carlo code was demonstrated.

Acknowledgements Our profound gratitude and appreciation go to the Egyptian and Japanese governments for supporting and financing this research work at the Egypt-Japan University of Science and Technology. Further appreciation goes to the Science and Technology Development Fund for the additional financial support (project ID: STDF-33397).

Authors contributions All authors contributed to the study conception and design. Material preparation, data collection and analysis were performed by JKB, ASGK, MAH and SAEM. The first draft of the manuscript was written by JKB and all authors commented on previous versions of the manuscript. All authors read and approved the final manuscript.

Declarations

Conflict of interest The authors declare that they have no competing interests.

References

1. R.M. Lokhande, V. Vinayak, S.V. Mukhamale et al., Gamma radiation shielding characteristics of various spinel ferrite nanocrystals: a combined experimental and theoretical investigation. RSC Adv. **11**, 7925–7937 (2021). https://doi.org/10.1039/d0ra08372k
2. J.K. Boahen, S.A.E. Mohamed, A.S.G. Khalil et al., Finite element formulation and simulation of gamma ray attenuation of single and multilayer materials using lead, Tungsten and EPDM. Mater. Sci. Forum. **1069**, 87–94 (2022). https://doi.org/10.4028/p-ol4895
3. R. Li, S. Liu, X. Zhang et al., Nuclides selection method for nuclear reactor shielding based on non-dominated sorting. Ann. Nucl. Energy. **182**, 109633 (2023). https://doi.org/10.1016/j.anucene.2022.109633
4. H. Hirayama, H. Nakashima, M. Morishima et al., Progress and prospects of calculation methods for radiation shielding. J. Nucl. Sci. Technol. **52**, 1339–1361 (2015). https://doi.org/10.1080/00223131.2015.1021283
5. O. Gencel, The application of artificial neural networks technique to estimate mass attenuation coefficient of shielding barrier. Int. J. Phys. Sci **4**, 743–751 (2009)
6. L. Deng, G. Li, B.Y. Zhang et al., A high fidelity general purpose 3-D Monte Carlo particle transport program JMCT3.0. Nucl. Sci. Tech. **33**, 108 (2022). https://doi.org/10.1007/s41365-022-01092-0
7. C.J. Werner, J. Armstrong, F.B. Brown, et al., MCNP user's manual code version 6.2. Los Alamos Natl. Lab., (2017). p. 746
8. Geant4 Collaboration. Introduction to Geant4 release 11.0 geant4 collaboration. (2021)
9. W. Nelson, Y. Namito, The EGS4 code system: solution of gamma-ray and electron transport problems. Int. Conf. Supercomput. Nucl. Appl. (1990)
10. A. Cook, G.C. Meggitt, Radiological protection. Energy Dig. **8**, 16–19 (1979). https://doi.org/10.4324/9780203020746-18
11. D. Trubey, New gamma-ray buildup factor data for point kernel calculations. (1988)
12. A. Kratsios, The universal approximation property. Ann. Math. Artif. Intell. **89**, 435–469 (2021). https://doi.org/10.1007/s10472-020-09723-1
13. V. Ljubenov, R.D. Simović, S. Marković et al., Total reflection coefficients of low-energy photons presented as universal functions. Nucl. Technol. Radiat. Prot. **25**, 100–106 (2010). https://doi.org/10.2298/NTRP1002100L
14. J. Wood, *Computational methods in reactor shielding*, 1st edn. (Pergamon Press, New York, 1982)
15. T.Y. Huang, Z.G. Li, K. Wang et al., Hybrid windowed networks for on-the-fly Doppler broadening in RMC code. Nucl. Sci. Tech. **32**, 1–13 (2021). https://doi.org/10.1007/s41365-021-00901-2
16. M. Salman, Evaluation of the absorption, scattering and overall probability of gamma rays in lead and concrete. Interactions **4**, 191–199 (2021)
17. N. Tsoulfanidis, S. Landsberger, *Measurement & detection of radiation* (CRC Press, Boca Raton, 2015)
18. M. Sharifzadeh, H. Afarideh, H. Khalafi et al., A Matlab-based Monte Carlo algorithm for transport of gamma-rays in matter. Monte Carlo Methods Appl. **21**, 77–90 (2015). https://doi.org/10.1515/mcma-2014-0011
19. M.J. Berger, J.H. Hubbell, S.M. Seltzer, et al., XCOM: photon cross sections database. (1998)
20. A. Haghighat, *Monte Carlo methods for particle transport* (CRC Press, Boca Raton, 2016)

21. A.F. Bielajew, Fundamentals of the Monte Carlo method for neutral and charged particle transport. Sci. York, (2000)
22. E.D. Cashwell, C.J. Everett, A practical manual on the Monte Carlo method for random walk. (1957)
23. S. García-Pareja, A.M. Lallena, F. Salvat, Variance-reduction methods for Monte Carlo simulation of radiation transport. Front. Phys. **9**, 1–13 (2021). https://doi.org/10.3389/fphy.2021.718873
24. R. Dastres, M. Soori, Artificial neural network systems. Int. J. Imaging Robot. **21**, 13–25 (2021)
25. Y. Upadhyay, Introduction to feedforward neural networks. Towards. Data. Sci. (2019)
26. C. Li, Y. Song, Z. Zhang, et al., A novel and high-precision method for calculating the γ -ray build-up factor for multilayer shields. **2021**, 8860762 (2021). https://doi.org/10.1155/2021/8860762
27. A. Quesada, 5 algorithms to train a neural network. Artificial Intelligence Techniques, Ltd, 2022. https://www.neuraldesigner.com/blog/5_algorithms_to_train_a_neural_network (accessed Jun. 05, 2022)
28. S. Basterrech, S. Mohammed, G. Rubino et al., Levenberg–Marquardt training algorithms for random neural networks. Comput. J. **54**, 125–135 (2011). https://doi.org/10.1093/comjnl/bxp101
29. U.T. Lin, S.H. Jiang, A dedicated empirical formula for γ-ray buildup factors for a point isotropic source in stratified shields. Radiat. Phys. Chem. **48**, 389–401 (1996). https://doi.org/10.1016/0969-806X(95)00461-6
30. A. Kiyani, A.A. Karami, M. Bahiraee et al., Calculation of gamma buildup factors for point sources. Adv. Mater. Res. **2**, 93–98 (2013). https://doi.org/10.12989/amr.2013.2.2.093
31. ANSI/ANS-6.4.3,Gamma-ray attenuation coefficients and buildup factors for engineering materials. Am. Nuclear Soc. (1991)
32. A. Das, T. Singh, Development of a new Monte Carlo based transport code to calculate photon exposure build-up factors in various shielding arrangements. Radiat. Phys. Chem. **194**, 110028 (2022). https://doi.org/10.1016/j.radphyschem.2022.110028
33. E. Aslani-amoli, Dissertation. University of Missori-ROLLA. (1973)